# Deriving inherent optical properties from water color: a multiband quasi-analytical algorithm for optically deep waters

ZhongPing Lee, Kendall L. Carder, and Robert A. Arnone

For open ocean and coastal waters, a multiband quasi-analytical algorithm is developed to retrieve absorption and backscattering coefficients, as well as absorption coefficients of phytoplankton pigments and gelbstoff. This algorithm is based on remote-sensing reflectance models derived from the radiative transfer equation, and values of total absorption and backscattering coefficients are analytically calculated from values of remote-sensing reflectance. In the calculation of total absorption coefficient, no spectral models for pigment and gelbstoff absorption coefficients are used. Actually those absorption coefficients are spectrally decomposed from the derived total absorption coefficient in a separate calculation. The algorithm is easy to understand and simple to implement. It can be applied to data from past and current satellite sensors, as well as to data from hyperspectral sensors. There are only limited empirical relationships involved in the algorithm, and they are for less important properties, which implies that the concept and details of the algorithm could be applied to many data for oceanic observations. The algorithm is applied to simulated data and field data, both non-case$_1$, to test its performance, and the results are quite promising. More independent tests with field-measured data are desired to validate and improve this algorithm. 

*OCIS codes:* 010.4450, 290.5850, 280.0280.

## 1. Introduction

Absorption and backscattering coefficients are inherent optical properties.[1] Combined with downwelling light from the Sun and sky, they determine the appearance of water color, which is normally measured by the water-leaving radiance or remote-sensing reflectance[2] (ratio of water-leaving radiance to above-surface downwelling irradiance). As inherent optical properties are directly linked to the constituents in the water, their values are used to determine the type of water, subsurface light intensity, solar heat flux with depth, turbidity, pigment concentration, and sediment loading to name a few applications.[2–6] Methods to accurately retrieve these optical properties remotely have been under investigation for several decades, and algorithms from empirical to full-spectral optimization have been proposed.[2,7–31]

Empirical algorithms[2,7–22] apply simple or multiple regressions between the property of interest and the ratios (or values) of irradiance reflectance[7,22] or remote-sensing reflectance[2,11] ($r_{rs}$, see Table 1 for symbols and definitions used in this paper). They do not require a full understanding of the relationship between $r_{rs}$ and the properties. Because of the nature of regression, however, these kinds of algorithm are generally only appropriate to waters with characteristics similar to those used in the algorithm development. Their applicability then can be quite limited and can result in significant errors. More importantly, because of the wide variation of optical properties found for global waters, one empirical function cannot fit all waters, unless the waters are restricted to case$_1$ conditions[7] where all optical properties co-vary with chlorophyll concentrations. The biggest advantages of this kind of algorithm are the simplicity and rapidity in data processing, which are important for the retrieval of information from large data sets such as satellite images.

The semianalytical algorithms,[23–30] including the spectral optimization approach,[23,27–29] are based on

When this research was performed, Z. Lee and K. L. Carder were with the College of Marine Science, University of South Florida, St. Petersburg, Florida 33701. Z. P. Lee (zplee@nrlssc.navy.mil) and R. A. Arnone are now with the U.S. Naval Research Laboratory, Code 7333, Stennis Space Center, Mississippi 39529.

Received 21 February 2002; revised manuscript received 11 June 2002.

0003-6935/02/275755-18$15.00/0

Table 1. Symbols and Definitions

| Symbol | Description | Unit |
|---|---|---|
| $a$ | Absorption coefficient of the total, $a_w + a_\phi + a_g$ | $m^{-1}$ |
| $a_\phi$ | Absorption coefficient of phytoplankton pigments | $m^{-1}$ |
| $a_g$ | Absorption coefficient of gelbstoff and detritus | $m^{-1}$ |
| $a_w$ | Absorption coefficient of pure seawater | $m^{-1}$ |
| $a(\lambda)^{[555]}$ | Total absorption coefficient at λ from the QAA-555 | $m^{-1}$ |
| $a(\lambda)^{[640]}$ | Total absorption coefficient at λ from the QAA-640 | $m^{-1}$ |
| $b_{bp}$ | Backscattering coefficient of suspended particles | $m^{-1}$ |
| $b_{bw}$ | Backscattering coefficient of pure seawater | $m^{-1}$ |
| $b_b$ | Backscattering coefficient of the total, $b_{bw} + b_{bp}$ | $m^{-1}$ |
| $A$, $B$ | Model parameters for phytoplankton specific-absorption coefficient at 440 nm | |
| $[C]$ | Pigment concentration | $mg/m^3$ |
| $Y$ | Spectral power for particle backscattering coefficient | |
| $q_n^{\text{der}}$ | Algorithm-derived value | |
| $q_n^{\text{true}}$ | True value | |
| $R_{\text{rs}}$ | Above-surface remote-sensing reflectance | $sr^{-1}$ |
| $r_{\text{rs}}$ | Below-surface remote-sensing reflectance | $sr^{-1}$ |
| $S$ | Spectral slope for gelbstoff absorption coefficient | $nm^{-1}$ |
| $u$ | Ratio of backscattering coefficient to the sum of absorption and backscattering coefficients, $b_b/(a + b_b)$ | |
| $\lambda_0$ | Reference wavelength | nm |
| $\zeta$ | $a_\phi(410)/a_\phi(440)$ | |
| $\xi$ | $a_g(410)/a_g(440)$ | |

solutions to the radiative transfer equation. These algorithms can be applied to different water types, and retrieval accuracy is often much better than those of empirical algorithms.[23,31] The performance of these algorithms, however, relies on accurate spectral models for the absorption coefficients of each individual constituent presented in the water, such as pigments, gelbstoff [also called colored dissolved organic matter (CDOM)], or suspended sediments. The accuracy of these models will affect the accuracy of remote-sensing retrievals. In addition, the optimization procedure is time-consuming,[31] which limits its applicability in the processing of large data sets, such as satellite images.

In this study, for waters of open ocean and coastal areas, we develop a multiband quasi-analytical algorithm (QAA) for retrieving the absorption and backscattering coefficients from remote-sensing reflectance of optically deep waters. Furthermore, the derived total absorption coefficient is spectrally decomposed into the contributions of phytoplankton pigments and gelbstoff. The algorithm is based on the relationship between $r_{\text{rs}}$ and the inherent optical properties of water derived from the radiative transfer equation. In the derivation of the total absorption coefficient, there are no spectral models involved for the absorption coefficients of pigments and gelbstoff. Instead, the derived total absorption coefficient is further decomposed spectrally into the absorption coefficients of pigments and gelbstoff when necessary. The algorithm is applied to both simulated and field-measured non-case$_1$ data to test its performance. We show that its accuracy is similar to that of optimization, but calculation efficiency is similar to that of empirical algorithms.

This QAA can be quickly applied to data from past and current ocean-color satellite sensors, such as the Coastal Zone Color Scanner (CZCS), the sea-viewing wide field-of-view sensor (SeaWiFS), and the moderate-resolution imaging spectroradiometer (MODIS), as these sensors have only a few spectral bands in the visible domain. This algorithm can also be applied to hyperspectral airborne sensors or future hyperspectral satellite sensors.

## 2. Multiband Quasi-Analytical Algorithm

### A. General Concept

Figure 1, the schematic flow chart, presents the concept of the level-by-level derivation and the QAA. The left side of Fig. 1 lays out the levels from remote-sensing reflectance to the concentrations of phytoplankton pigments or CDOM. The right side shows the QAA used to derive the particle backscattering and total absorption coefficients. Our approach here is to calculate optical properties first[32] and in a level-by-level scheme instead of solving all in one stroke, such as the optimization approach[23,27–29] or the linear matrix inversion.[25] This way the accuracy for returns on a higher level (level 1, for example) has little or no dependence on how to handle the properties on the lower levels (level 2 or 3, for example), as it should be in water-color inversion. The methods to derive level 1 data from level 0 data and level 2 data from level 1 data are presented here. Converting pigment and gelbstoff absorption coefficients to their corresponding concentrations can be found in Carder *et al.*[26] and Roesler and Perry.[27]

In general, on the basis of theoretical analyses[22] and numerical simulations[33–38] of the radiative transfer equation, $r_{\text{rs}}$ is a function of the absorption and backscattering coefficients. Specifically, measure-

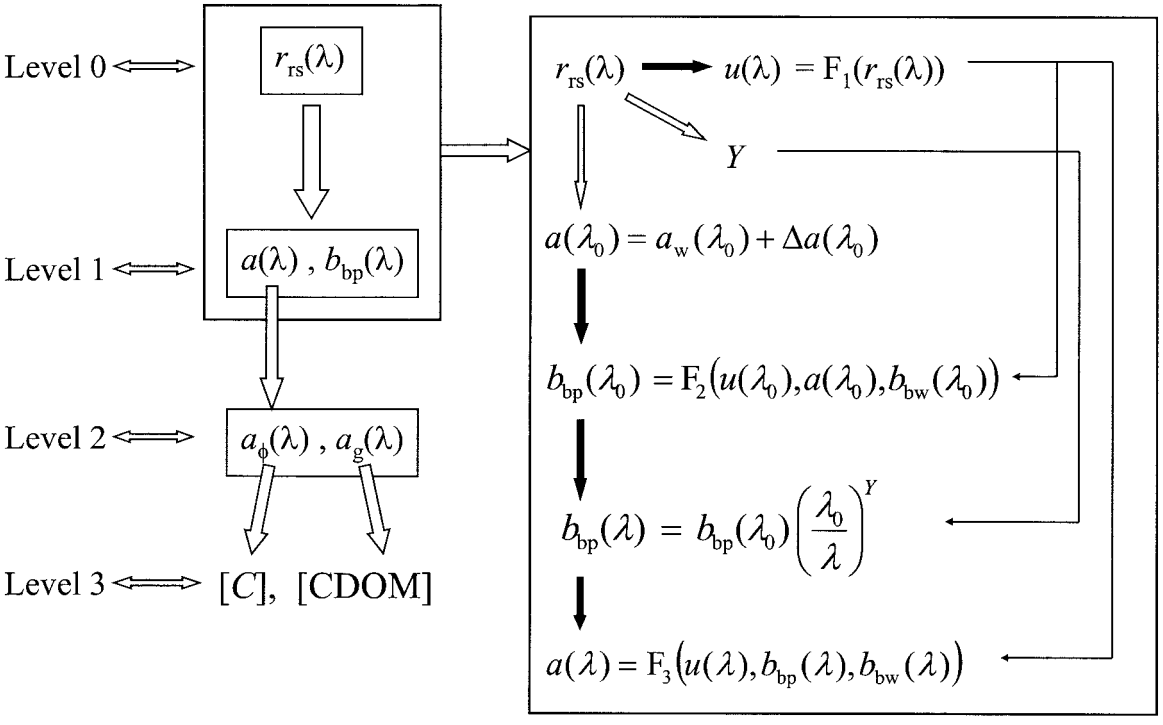


Fig. 1. Concept and schematic flow chart of the level-by-level ocean-color remote sensing and the QAA.

ment of $r_{rs}$ is a measure of the ratio $u$ of the backscattering coefficient to the sum of absorption and backscattering coefficients, with an error of ~2% to ~10%. This accuracy depends on the accuracy of one knowing the particle phase function of the water under study and the accuracy of one modeling $r_{rs}$ as a function of $u$. Applying existing $r_{rs}$ models, values of $u$ can be calculated analytically from values of $r_{rs}$. Because $u$ is just a ratio of the backscattering coefficient to the sum of absorption and backscattering coefficients, then knowledge of the absorption coefficient enables us to calculate the backscattering coefficient, or vice versa.

To illustrate the derivation of $u$ from $r_{rs}$, the Gordon *et al.*[33] formula is used here:

$$r_{rs}(\lambda) = g_0 u(\lambda) + g_1[u(\lambda)]^2, \quad (1)$$

with

$$u = \frac{b_b}{a + b_b}. \quad (2)$$

Here $a$ is the total absorption coefficient and $b_b$ is the total backscattering coefficient. $\lambda$ is the wavelength (which may not be shown for brevity). $b_b$ is normally expressed as[2,7] $b_b = b_{bw} + b_{bp}$, with $b_{bw}$ the backscattering coefficients for water molecules. $b_{bp}$ is the backscattering coefficients for nonmolecules, collectively called the backscattering coefficients of suspended particles, which actually may include the contributions of virus[39] or bubbles[40] in natural waters.

For nadir-viewed $r_{rs}$, Gordon *et al.*[33] found that $g_0 \approx 0.0949$ and $g_1 \approx 0.0794$ for oceanic case$_1$ waters. Recently Lee *et al.*[34] suggested that $g_0$ of 0.084 and $g_1$ of 0.17 work better for higher-scattering coastal waters. Actually the values of $g_0$ and $g_1$ may vary with particle phase function,[38] which is not known remotely. Values of $g_0$ and $g_1$, however, need to be predetermined as in any semianalytical algorithm. Without preference and aimed at applying the QAA to both coastal and open-ocean waters, we used the averaged $g_0$ and $g_1$ values of Gordon *et al.*[33] and Lee *et al.*,[34] which are $g_0 = 0.0895$ and $g_1 = 0.1247$.

From Eq. (1),

$$u(\lambda) = \frac{-g_0 + [(g_0)^2 + 4g_1 r_{rs}(\lambda)]^{1/2}}{2g_1}. \quad (3)$$

Other formulas or procedures for the derivation of $u$ can be applied on the basis of existing models.[34–38] As long as $u(\lambda)$ is accurately derived from $r_{rs}(\lambda)$, the following steps are the same.

As $u$ is a simple ratio of $b_b$ to $(a + b_b)$, knowing $a$ will lead to

$$b_b = \frac{ua}{1 - u}, \quad (4)$$

or knowing $b_b$ will lead to

$$a = \frac{(1 - u)b_b}{u}. \quad (5)$$

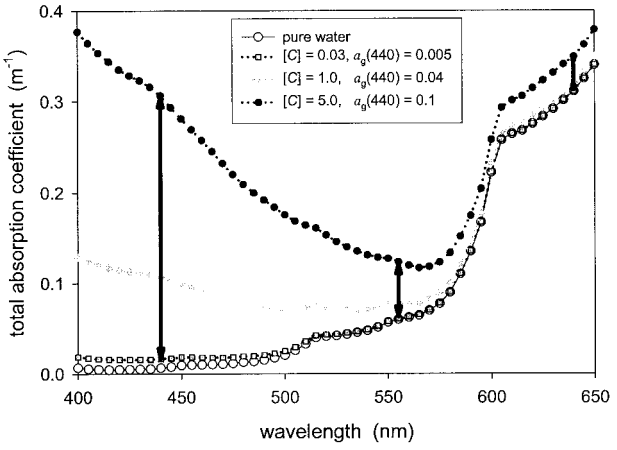


Fig. 2. Examples of $a(\lambda)$ variations at different wavelengths.

For each wavelength, the total absorption coefficient can be expressed as

$$a(\lambda) = a_w(\lambda) + \Delta a(\lambda), \tag{6}$$

where $a_w$ is the absorption coefficient of pure water and $\Delta a$ is the contribution that is due to dissolved and suspended constituents. We note that, at longer wavelengths (>550 nm), $\Delta a(\lambda)$ is quite small, with $a(\lambda)$ dominated by the values of $a_w(\lambda)$, especially for oligotrophic and mesotrophic waters. Figure 2 presents examples of $a(\lambda)$ variations. In these examples, a 20-fold $a(440)$ variation corresponds to a factor of 2 variation for $a(555)$ and just a fractional variation for $a(640)$. These facts suggest that, if a reference wavelength ($\lambda_0$) is found where $r_{rs}(\lambda_0)$ from elastic scattering can be accurately measured and $a(\lambda_0)$ can be well estimated, then $b_b$ at $\lambda_0$ can be calculated from Eq. (4). As $b_b$ is a simple sum of $b_{bw}$ and $b_{bp}$ (Refs. 2 and 7) and the value of $b_{bw}(\lambda)$ is already known,[41] then the $b_{bp}$ value at $\lambda_0$ is calculated.

The wavelength dependence of $b_{bp}(\lambda)$ is normally expressed as[2,22,42,43]

$$b_{bp}(\lambda) = b_{bp}(\lambda_0)\left(\frac{\lambda_0}{\lambda}\right)^Y. \tag{7}$$

This suggests that, if the power value $Y$ is known or can be estimated from remote-sensing measurements, then $b_{bp}$ at any wavelength can be calculated. If we place this calculated $b_{bp}(\lambda)$ value along with the $b_{bw}(\lambda)$ value into Eq. (5), then the total absorption coefficient at that wavelength can be calculated analytically from $r_{rs}(\lambda)$.

As shown above [Eqs. (1)–(7)], there are no spectral models involved for the absorption coefficients of pigments or gelbstoff. As a matter of fact, the simple math functions such as the log-normal shape used by Lee *et al.*[28] and the Gaussian shape used by Hoge and Lyon[25] cannot accurately simulate all the spectral shapes of the pigment absorption coefficient observed in the field. The simplification of the QAA here reduced the potential errors from inaccurate spectral models of pigment and gelbstoff absorption coefficients in the retrieval of the total absorption coefficient.

Using 555 nm as the reference wavelength ($\lambda_0$), in Table 2 we detail the steps of applying the QAA. This $\lambda_0$ can be changed to shorter or longer wavelengths, such as 640 nm that is shown in Subsection 4.A. for high-absorbing waters, to obtain better measurement of $r_{rs}(\lambda_0)$ and a better estimate of $a(\lambda_0)$. For such cases, small adjustments are required accordingly, but the analytical calculation scheme in Fig. 1 and Table 2 will remain the same. Table 2 also summarizes the optical properties involved, the mathematical formula for each calculation, the order of importance of each property, and the character of each step. Explanations and comments are provided in Subsection 2.B.

**Table 2. Steps of the QAA to Derive Absorption and Backscattering Coefficients from Remote-Sensing Reflectance with 555 nm as the Reference Wavelength**

| Step | Property | Math Formula | Order of Importance | Approach |
|---|---|---|---|---|
| 0 | $r_{rs}$ | $=R_{rs}/(0.52 + 1.7R_{rs})$ | 1st | Semianalytical |
| 1 | $u(\lambda)$ | $= \dfrac{-g_0 + [(g_0)^2 + 4g_1 r_{rs}(\lambda)]^{1/2}}{2g_1}$ | 1st | Semianalytical |
| 2 | $a(555)$ | $=0.0596 + 0.2[a(440)_i - 0.01]$, $a(440)_i = \exp(-2.0 - 1.4\rho + 0.2\rho^2)$, $\rho = \ln[r_{rs}(440)/r_{rs}(555)]$ | 2nd | Empirical |
| 3 | $b_{bp}(555)$ | $= \dfrac{u(555)a(555)}{1 - u(555)} - b_{bw}(555)$ | 1st | Analytical |
| 4 | $Y$ | $= 2.2\left\{1 - 1.2\exp\left[-0.9\dfrac{r_{rs}(440)}{r_{rs}(555)}\right]\right\}$ | 2nd | Empirical |
| 5 | $b_{bp}(\lambda)$ | $= b_{bp}(555)\left(\dfrac{555}{\lambda}\right)^Y$ | 1st | Semianalytical |
| 6 | $a(\lambda)$ | $= \dfrac{[1 - u(\lambda)][b_{bw}(\lambda) + b_{bp}(\lambda)]}{u(\lambda)}$ | 1st | Analytical |

### B. Derivation of Total Absorption and Backscattering Coefficients

Step 0 converts above-surface remote-sensing reflectance spectra $R_{rs}$ to below-surface spectra $r_{rs}$ because satellites and many other sensors measure remote-sensing reflectance from above the surface. If measurement is made below the surface, this step can be skipped. For the $R_{rs}$ to $r_{rs}$ conversion,[33,44]

$$r_{rs} = \frac{R_{rs}}{T + \gamma Q R_{rs}}, \tag{8}$$

where $T = t_- t_+ / n^2$ with $t_-$ the radiance transmittance from below to above the surface and $t_+$ the irradiance transmittance from above to below the surface, and $n$ is the refractive index of water. $\gamma$ is the water-to-air internal reflection coefficient. $Q$ is the ratio of upwelling irradiance to upwelling radiance evaluated below the surface. For a nadir-viewing sensor and the remote-sensing domain,[35] $Q$, in general, ranges between 3 and 6.[35] As $R_{rs}$ is small (in the range of 1% at the high end[31]) for most oceanic and coastal waters, the variation of the $Q$ value has only little influence on the conversion between $R_{rs}$ and $r_{rs}$. From calculated HYDROLIGHT[45] $R_{rs}$ and $r_{rs}$ values, it is found that $T \approx 0.52$ and $\gamma Q \approx 1.7$ for optically deep waters and a nadir-viewing sensor.

Knowing $r_{rs}$, values of $u$ can be quickly calculated, for example, with Eq. (3) as shown in step 1.

Step 2 estimates $a(555)$ empirically. Depending on the sensor's configurations and sensitivities to changes of water properties, there could be many ways to perform this estimation. As an example, we use here the Austin and Petzold[8] approach, with parameters adjusted for the absorption coefficient instead of the diffuse attenuation coefficient. The initial estimation of $a(440)_i$ here is solely for the empirical estimation of $\Delta a(555)$ as $a(440)$ is sensitive to the change of water properties. $a(440)_i$ is calculated on the basis of an earlier study[11] but is adapted to bands at 440 and 555 nm as in Mueller and Trees.[10] As pointed out above and discussed in Subsection 4.A, a simple empirical algorithm such as this one may not accurately estimate $a(440)_i$ for non-case$_1$ waters; in turn $\Delta a(555)$ may not be accurate either. However, as $\Delta a(555)$ is small compared with $a(555)$ for most oceanic waters (see Fig. 2), the errors of $\Delta a(555)$ will have a smaller impact on the accuracy of $a(555)$. When the errors for $a(555)$ are no longer tolerable, such as near the shore or for river plume waters, $\lambda_0$ has to be shifted to a longer wavelength by this approach.

Step 3 calculates $b_{bp}(555)$ from $r_{rs}(555)$ and $a(555)$ on the basis of Eq. (4).

Step 4 estimates the wavelength dependence (value of $Y$) of the particle backscattering coefficient. A value for $Y$ is required if we want to calculate particle backscattering coefficients from one wavelength to another wavelength by Eq. (7). Historically, researchers set $Y$ values based on the location of the water sample,[13,29] such as 0 for coastal waters and 2.0 for open-ocean waters. Here we used the empirical algorithm of Lee *et al.*[46] to estimate the $Y$ value, but adapted it for bands at 440 and 555 nm.

Step 5 computes the particle backscattering coefficients at other wavelengths given the values of $Y$ and $b_{bp}(555)$ by use of Eq. (7).

Step 6 completes the calculation for $a(\lambda)$ given the values of $u(\lambda)$ (step 1) and $b_{bp}(\lambda)$ (step 5) based on Eq. (5).

As shown from step 1 to step 6, there are two semianalytical expressions [Eqs. (1) and (7)] and two empirical formulas (steps 2 and 4) used for the entire process. Certainly the accuracy of the final calculated $a(\lambda)$ relies on the accuracy of each individual step. The semianalytical expressions are currently widely accepted and used, their improvements are out of the scope of this study, and Eqs. (1) and (7) could be simply replaced by better expressions when available. The empirical formulas used either provide estimates at the reference wavelength [$a(555)$] or estimates of less important quantities (values of $Y$, for example). As shown in Table 2, these properties have only second-order importance.

The order of importance for a property is based on its range of variation and its influence on the final output. Values of $r_{rs}$, for example, vary widely and have a great influence on the final results, so they are of first-order importance. Values of $a(555)$, however, vary over a much narrower range except near shore (see Fig. 2) and have only a small influence on the final results, so $a(555)$ is of second-order importance. Although values of $Y$ vary over a range of 0–2.0 or so, they have a relatively small influence on the final results because this value is used in a power law on the ratio of wavelengths for the particle backscattering coefficient. For example, for the expression $(555/440)^Y$, a change of $Y$ from 0 to 2.0 merely changes the expression from 1.0 to 1.59. If the true $Y$ value is 1.0 but an estimate of 2.0 is used, this will make the calculated $b_{bp}(440)$ 21% higher than it should be. On the other hand, for the same true $Y$ value of 1.0 but an estimate of 0.0 is used, this will make the calculated $b_{bp}(440)$ 26% lower than it should be. These errors will be transferred to the calculated total absorption coefficient at 440 nm, but, as shown, the errors are in a limited range.

The quantities with second-order importance, however, do affect the end products, and further improvements to the end products can be achieved if the secondary quantities are better estimated with regional and seasonal information, or with improved algorithms.

### C. Decomposition of the Total Absorption Coefficient

The data processing can be stopped here if the interest of remote sensing is on the total absorption coefficient or the particle backscattering coefficient. For many remote-sensing applications, however, it is also desired to know the absorption coefficients for phytoplankton pigment [$a_\phi(\lambda)$] and gelbstoff [$a_g(\lambda)$] because these properties can be converted to concentrations of chlorophyll[26] or CDOM,[27] respec-

Table 3. Steps to Decompose the Total Absorption to Phytoplankton and Gelbstoff Components, with Bands at 410 and 440 nm

| Step | Property | Math Formula | Order of Importance | Approach |
|---|---|---|---|---|
| 7 | $\zeta = a_\phi(410)/a_\phi(440)$ | $= 0.71 + \dfrac{0.06}{0.8 + r_{rs}(440)/r_{rs}(555)}$ | 2nd | Empirical |
| 8 | $\xi = a_g(410)/a_g(440)$ | $= \exp[S(440–410)]$ | 2nd | Semianalytical |
| 9 | $a_g(440)$ | $= \dfrac{[a(410) - \zeta a(440)]}{\xi - \zeta} - \dfrac{[a_w(410) - \zeta a_w(440)]}{\xi - \zeta}$ | 1st | Analytical |
| 10 | $a_\phi(440)$ | $= a(440) - a_g(440) - a_w(440)$ | 1st | Analytical |

tively. For this latter purpose, data processing continues.

It is much more challenging to separate $a_\phi(\lambda)$ and $a_g(\lambda)$ from the total absorption coefficient as the total absorption is at least a sum of pure water, phytoplankton pigment, and gelbstoff. It is impossible to partition the total absorption if the $a(\lambda)$ value is known only at one wavelength, except perhaps for case$_1$ waters.[7] For non-case 1 situations, to solve for the two unknowns, at least the $a(\lambda)$ value and the spectral relations of $a_\phi(\lambda)$ and $a_g(\lambda)$ at two or more bands are required. Table 3 extends the calculations for this purpose. As in other semianalytical algorithms,[31] there is no separation of the absorption coefficient of detritus from that of gelbstoff, so the derived $a_g(440)$ here is actually the sum of detritus and gelbstoff absorption coefficients. Lee[47] has developed a simple empirical algorithm for that separation.

Basically, the approach here assumes that $a(\lambda)$ values at both 410 and 440 nm are calculated by the steps in Table 2. For the decomposition, two more values must be known: $\zeta[=a_\phi(410)/a_\phi(440)]$ and $\xi[=a_g(410)/a_g(440)]$. $\zeta$ has been either related to chlorophyll concentration[48] or pigment absorption at a wavelength.[23–29] As chlorophyll concentration or pigment absorption are still unknowns, the value of $\zeta$ cannot be derived by use of such approaches. Here, the value of $\zeta$ is estimated in step 7 by use of the spectral ratio of $r_{rs}(440)/r_{rs}(555)$ based on the field data of Lee *et al.*[11] The value of $\xi$ is calculated in step 8 when we assume a spectral slope of 0.015 $nm^{-1}$.[49] Note that the values of $\zeta$ and $\xi$ may vary based on the nature of waters under study, such as pigment composition,[50] humic versus fulvic acids,[51] and abundance of detritus.[52] Local information or improved algorithms to calculate $\zeta$ and the parameter $S$ (involved in the calculation of $\xi$) will improve the separation of the absorption coefficients of pigment and gelbstoff.

When the values of $a(410)$, $a(440)$, $\zeta$, and $\xi$ are known,[2,22,26]

$$\begin{cases} a(410) = a_w(410) + \zeta a_\phi(440) + \xi a_g(440), \\ a(440) = a_w(440) + a_\phi(440) + a_g(440). \end{cases} \quad (9)$$

Solving this set of simple algebraic equations provides

$$\begin{cases} a_g(440) = \dfrac{[a(410) - \zeta a(440)] - [a_w(410) - \zeta a_w(440)]}{\xi - \zeta}, \\ a_\phi(440) = a(440) - a_w(440) - a_g(440). \end{cases} \quad (10)$$

And, if values of $a(\lambda)$, $a_g(440)$, and $S$ are known, the $a_\phi(\lambda)$ spectrum can then be easily calculated: $a_\phi(\lambda) = a(\lambda) - a_w(\lambda) - a_g(440)\exp[-S(\lambda - 440)]$. Unlike earlier approaches,[23,27–29] the derivation of $a_\phi(\lambda)$ here requires no prior knowledge of what kind of phytoplankton pigments might be in the water or of a spectral model for $a_\phi(\lambda)$ at all wavelengths, although we do need to know $a_\phi(410)/a_\phi(440)$.

### 3. Data to Test the Quasi-Analytical Algorithm

To test the performance of the QAA, we applied it to both simulated and field-measured data sets, neither of which are case$_1$ dependent. Simulated data have no involvement in the measurements; the errors associated with the measurement processes are avoided. Then the differences between retrievals and inputs are solely due to the algorithm.

#### A. Simulated Data

To create a valid data set, we varied the pigment concentration $[C]$, as in Sathyendranath *et al.*,[22] and other bio-optical parameters in a way that generally mimics those found in the natural field. The following provides details about the data simulation. It would be better to use a numerical simulation technique such as Monte Carlo[33,35] or HYDROLIGHT[45] to create a simulated data set. However, because of the wide variation of water properties in the field, it is quite time-consuming to create a large case$_2$ data[7] set with such numerical techniques. Without losing generality regarding the QAA, we used Eq. (1) to replace the tedious radiative transfer computations. Later the QAA is applied to $r_{rs}$ values with added noise. These $r_{rs}$ values are then closer to the data from field measurements or from satellite sensors.

Values of absorption and backscattering coeffi-

cients are needed to create $r_{rs}$ by use of Eqs. (1) and (2)[2,22,42,52]:

$$a(\lambda) = a_w(\lambda) + a_\phi(\lambda) + a_g(\lambda),$$
$$b_b(\lambda) = b_{bw}(\lambda) + b_{bp}(\lambda). \quad (11)$$

Values for $a_w(\lambda)$ and $b_{bw}(\lambda)$ are already known.[41,53] We used the following bio-optical models[33,48,54,55] to create optical data sets that simulate oceanic and coastal waters:

$$a_\phi(440) = (A[C]^{-B})[C],$$
$$a_g(440) = p_1 a_\phi(440),$$
$$b_{bp}(555) = \{0.002 + 0.02[0.5 - 0.25\log([C])]\}p_2[C]^{0.62}. \quad (12)$$

Furthermore,

$$a_\phi(\lambda) = \{a_0(\lambda) + a_1(\lambda)\ln[a_\phi(440)]\}a_\phi(440),$$
$$a_g(\lambda) = a_g(440)\exp[-S(\lambda - 440)],$$
$$b_{bp}(\lambda) = b_{bp}(555)\left(\frac{555}{\lambda}\right)^Y, \quad (13)$$

where values for $a_0(\lambda)$ and $a_1(\lambda)$ are known.[56] Note that here $[C]$ is used only as a free parameter for designation of a wide range of absorption and backscattering values.

For case$_1$ waters,[33,54] $p_1 \approx 0.5$, $p_2 \approx 0.3$, $Y \approx 1.0$; and average $A$ and $B$ values are 0.0403 and 0.332 (Ref. 48) so that all optical properties co-vary with $[C]$ values, and only one fixed $r_{rs}(\lambda)$ spectrum will be created for a $[C]$ value. It is found in the field, however, that different $r_{rs}(\lambda)$ spectra exist for the same $[C]$ values. To accommodate such observations, we kept $B = 0.332$ and perturbed the other case$_1$ parameters in the following way:

$$A = 0.03 + 0.03\mathcal{R}_1,$$
$$p_1 = 0.3 + \frac{3.7\mathcal{R}_2 a_\phi(440)}{0.02 + a_\phi(440)},$$
$$p_2 = 0.1 + 0.8\mathcal{R}_3,$$
$$Y = 0.1 + \frac{1.5 + \mathcal{R}_4}{1 + [C]},$$
$$S = 0.013 + 0.004\mathcal{R}_5, \quad (14)$$

where $\mathcal{R}_1$, $\mathcal{R}_2$, $\mathcal{R}_3$, $\mathcal{R}_4$, and $\mathcal{R}_5$ are random values between 0 and 1. These kinds of perturbation make $A$, $p_1$, $p_2$, $Y$, and $S$ random values for each $[C]$ value, but fall in a range generally consistent with field observations.[37,48,55,57] In general, $A$ will range between 0.03 and 0.06, $p_1$ between 0.3 and 4.0, $p_2$ between 0.1 and 0.9, $Y$ between 0.1 and 2.5, and $S$ between 0.013 and 0.017 nm$^{-1}$. Also, to be consistent with field observations, the range for $p_1$ is narrower for low $[C]$ values (open ocean) and wider for high $[C]$ values (coastal), and $Y$ decreases with increasing $[C]$ values,[22] but in a random way for both $p_1$ and $Y$.

Values of $g_0$ and $g_1$ are also needed if we want to create $r_{rs}(\lambda)$ by Eq. (1). As discussed above, values of $g_0$ and $g_1$ are not constant; they may vary with phase function and scattering properties.[38] Because it is not known yet how they vary, we perturbed the $g_0$ and $g_1$ values in the following way:

$$g_0 = 0.084 + 0.011\mathcal{R}_6,$$
$$g_1 = 0.0794 + 0.0906\mathcal{R}_7. \quad (15)$$

$\mathcal{R}_6$ and $\mathcal{R}_7$ are random values between 0 and 1; thus $g_0$ will be randomly between 0.084 and 0.095 and $g_1$ randomly between 0.0794 and 0.17, within the reported values of Gordon *et al.*[33] and Lee *et al.*[34]

Therefore, for a $[C]$ value, there will be a range of $r_{rs}(\lambda)$ spectra simulated that are not just a function of $[C]$, but are also a function of the seven random values ($\mathcal{R}_{1-7}$). Figure 3(a) shows examples of $r_{rs}(\lambda)$ spectra for $[C] = 1.0$ mg/m$^3$, with $r_{rs}(\lambda)$ curves widely spread for the same $[C]$ value. For a $[C]$ range of 0.03–30 mg/m$^3$, 480 $r_{rs}$ spectra with wavelengths at 410, 440, 490, 555, and 640 nm were simulated. Figure 3(b) shows how the simulated $a(440)$ and $b_{bp}(555)$ values relate to the $[C]$ values of this data set, whereas Fig. 3(c) shows the $a_g(440)/a_\phi(440)$ variations. These wide variations clearly indicate that this data set is not case$_1$. Figure 3(d) shows how $[C]$ and $a(440)$ of this data set relate to the spectral ratio of $r_{rs}(490)/r_{rs}(555)$, a ratio often used in empirical chlorophyll algorithms.[16] The scatter of the data points indicates that it is hard to develop accurate empirical algorithms for $[C]$ or $a(440)$ simply on the basis of this ratio.

### B. Field Data

The data collected for waters around Baja California were used to see how the QAA-derived total absorption coefficient compared with AC9- (WET Labs, Inc.) measured values. This data set was collected in October 1999 during the Marine Optical Characterization Experiment 5, with a chlorophyll-*a* concentration range of 0.2–9.4 mg/m$^3$. For each station, remote-sensing reflectance was measured with a hand-held spectroradiometer from above the sea surface. The total absorption coefficients were measured through a vertically profiling of an AC9 instrument. The measurement method for remote-sensing reflectance can be found in Lee *et al.*[11,46] and Mueller *et al.*[58]

The vertical profiles of the total absorption coefficients (the Optical Group at Oregon State University) were obtained by an AC9 instrument attached to the Slow Descent Rate Optical Platform (WET Labs, Inc.). The profiling system was deployed with a winch wire, with descent rates typically of the order of 25–50 cm/s, providing submeter resolution. For details regarding the measurement and calibration of the AC9 instrument as well as the Slow Descent Rate Optical Platform see Pegau *et al.*[59] and Ref. 60.

Because remote sensing is a measure of the upper water column,[61] the absorption values from the vertical profiles were optically averaged by the approach

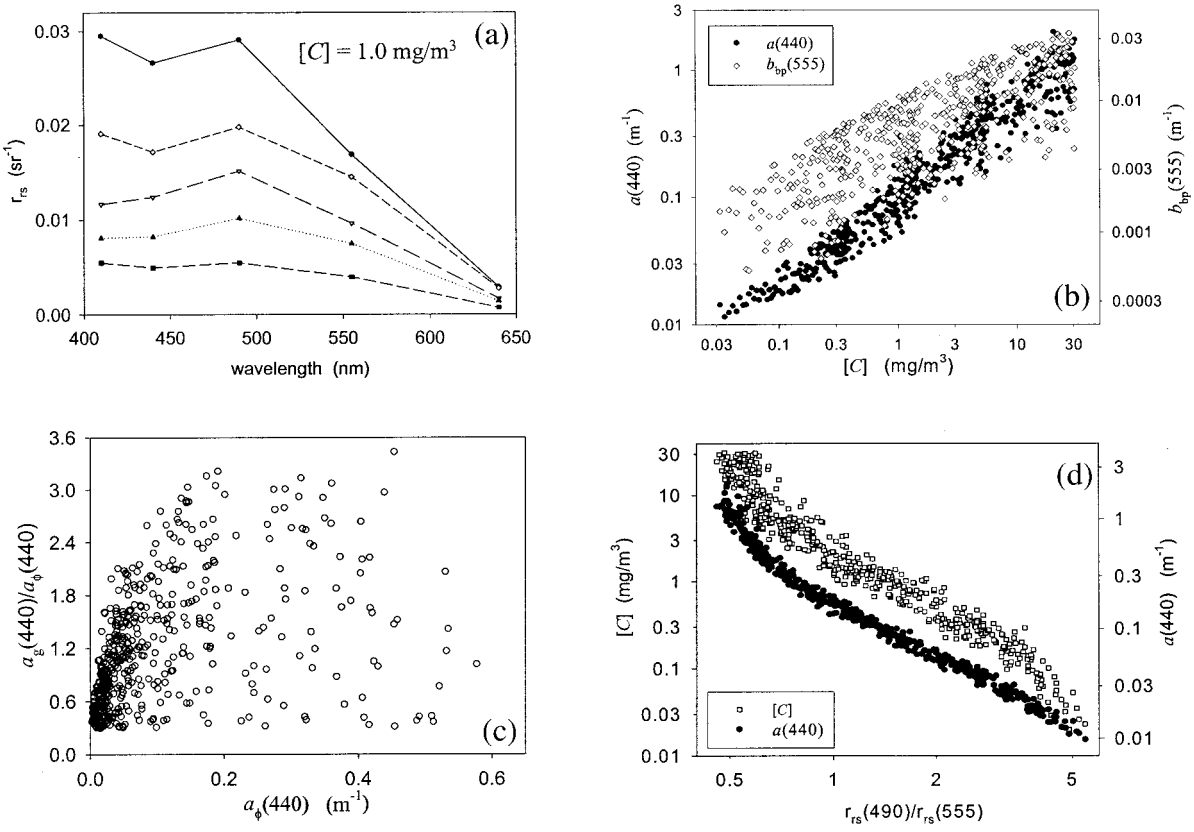


Fig. 3. Characteristics of the simulated data. (a) Possible $r_{rs}(\lambda)$ curves for $[C] = 1.0$ mg/m$^3$. (b) Values of $a(440)$ and $b_{bp}(555)$ versus pigment concentrations. (c) Values of $a_g(440)/a_\phi(440)$ versus values of $a_\phi(440)$. (d) Pigment concentration and $a(440)$ versus the spectral ratio of remote-sensing reflectance at 490 and 555 nm.

of Gordon[62] to make it comparable to those derived from color inversions.

## 4. Results and Discussion

Table 4 as well as Figs. 4–12 present the performance of the QAA. To be comparable with a few other inversion algorithms, Table 4 summarizes the percentage errors for $a(440)$, $b_{bp}(555)$, $a_\phi(440)$, and $a_g(440)$. A comparison at other wavelengths is presented either in Figs. 4–12 or in the text.

In Table 4, the two-band empirical algorithm is from Lee *et al.*,[11] which uses a spectral ratio of $r_{rs}(490)/r_{rs}(555)$. The spectral optimization algorithm is the same as used in Lee *et al.*[34,63] by use of available $r_{rs}$ at wavelengths 410, 440, 490, 555, and 640 nm.

The percentage error listed in Table 4 is calculated in the following way. First we calculated $\mathrm{RMSE}_{\log 10}$ (root-mean-square error in $\log_{10}$ scale) of quantity $q_n$ between the derived and the true values:

$$\mathrm{RMSE}_{\log 10} = \left\{ \frac{\sum_{n=1}^{N} [\log_{10}(q_n{}^{\mathrm{der}}) - \log_{10}(q_n{}^{\mathrm{true}})]^2}{N} \right\}^{1/2}. \tag{16}$$

Then the linear percentage error is

$$\varepsilon = 10^{\mathrm{RMSE}_{\log 10}} - 1. \tag{17}$$

**Table 4. Percentage Error ε between Derived and True Values of the Simulated Data**

| Data | Approach | $a(440)$ | $b_{bp}(555)$ | $a_\phi(440)$ | $a_g(440)$ |
|---|---|---|---|---|---|
| $a(440) < 0.3$ m$^{-1}$ | Two-band empirical[a] | 0.436 | | 0.333 | |
| | Optimization | 0.059 | 0.031 | 0.096 | 0.143 |
| | QAA-555 | 0.083 | 0.067 | 0.094 | 0.131 |
| | QAA-640 | 0.079 | 0.069 | 0.136 | 0.134 |
| Full range $0.01 < a(440) < 2.0$ m$^{-1}$ | Two-band empirical[a] | 0.426 | | 0.402 | |
| | Optimization | 0.061 | 0.039 | 0.176 | 0.138 |
| | QAA-555 | 0.143 | 0.186 | 0.166 | 0.175 |
| | QAA-640 | 0.076 | 0.073 | 0.123 | 0.130 |

[a]Lee *et al.*[11] empirical formula.

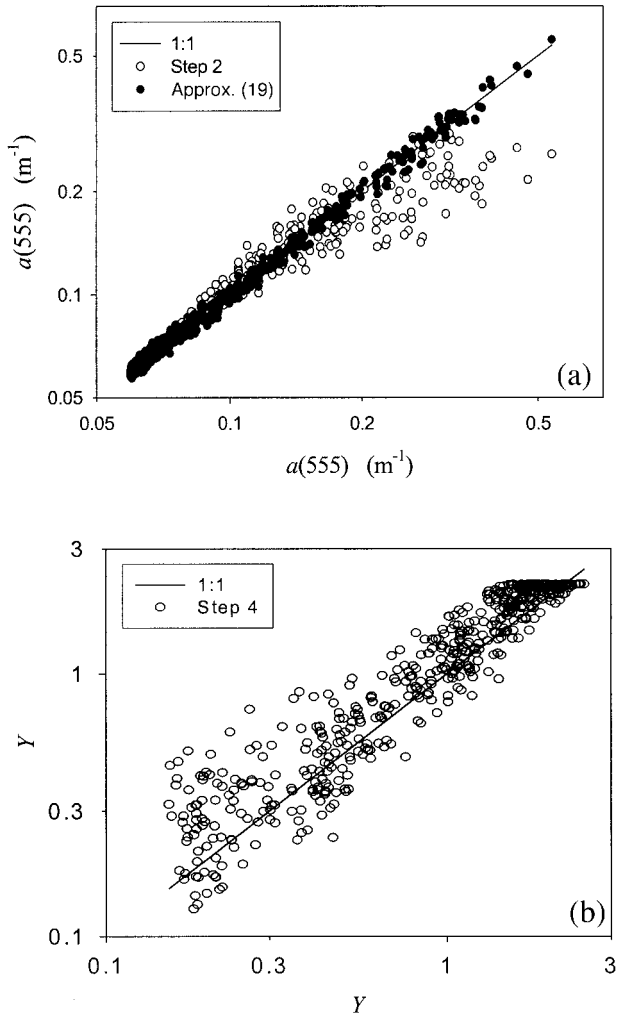


Fig. 4. (a) Empirically estimated $a(555)$ values versus true $a(555)$ values ($x$ axis). (b) Empirically estimated $Y$ values versus true $Y$ values ($x$ axis).

This kind of analysis puts equal emphasis on underestimates as well as on overestimates.

### A. Simulated Data

Figure 4(a) presents the empirically derived $a(555)$ values (from step 2, open circles) versus true values, and Fig. 4(b) presents empirically derived $Y$ values (step 4) versus true values. Apparently these two derivations, because of their empirical nature and the algorithms used, did not produce accurate returns [ε values are 16% for $a(555)$ and 35% for $Y$]. However, as discussed in Section 2, these two properties are of second-order importance, so the inaccuracy here does not affect the end results much. Actually, most of the $a(555)$ errors (underestimate) were at $a(555)$ greater than $\sim 0.2\ m^{-1}$ [which is a factor of 3 of the $a_w(555)$ value], which indicates less accuracy in the estimation of $a(555)$ for higher-absorbing waters, as discussed in Section 2.

Figure 5 compares the optical properties derived from the QAA with 555 nm (QAA-555) as the reference wavelength versus their true values, with Fig. 5(a) for the total absorption coefficient at 410, 440, and 490 nm; Fig. 5(b) for the particle backscattering coefficient at 555 nm; Fig. 5(c) for the pigment absorption coefficient at 410, 440, and 490 nm; and Fig. 5(d) for the gelbstoff absorption coefficient at 440 nm. Separation into $a_\phi(\lambda)$ and $a_g(\lambda)$ was achieved after we added the 410-nm band (Table 3) and used an $S$ value of $0.015\ nm^{-1}$. In the process, it is noticed that $\Delta a(555)$ in step 2 is derived from the coarse first estimate of $a(440)_i$, which involves some empirical parameters that may not well represent the waters under study. To overcome the uncertainties, the steps from step 2 to step 6 are repeated once, with $a(555)$ estimated (step 2) with $a(440)$ values from the first round of calculations. No improvement was found when additional iteration was applied, and apparently the results did not converge with more iterations.

Clearly the derived $a(\lambda)$ and $a_\phi(\lambda)$ match their true values well for the three wavelengths shown, especially for the clearer waters [$a(440) < 0.3\ m^{-1}$]. For the entire data set [$0.01 < a(440) < 2.0\ m^{-1}$], the linear percentage error (ε value) is 14.3% for $a(\lambda)$, 18.6% for $b_{bp}(555)$, 17.7% for $a_\phi(\lambda)$, and 17.5% for $a_g(440)$ values. For clearer waters [$a(440) < 0.3\ m^{-1}$, which encompass most oceanic waters[54]], the ε values for $a(\lambda)$, $b_{bp}(555)$, $a_\phi(\lambda)$, and $a_g(440)$ are 8.2%, 6.7%, 10.6%, and 13.1%, respectively. Not surprisingly, additional error is introduced when we further partition $a(\lambda)$ into $a_\phi(\lambda)$ and $a_g(\lambda)$ values because the parameters for $a_\phi(410)/a_\phi(440)$ and $a_g(410)/a_g(440)$ used in the algorithm (Table 3) may not match their input values ($S$ was randomly in a range of 0.013–$0.017\ nm^{-1}$ in the data simulation). Methods to better estimate the $S$ and $\zeta$ values are needed if we want to improve the $a_\phi(\lambda)$ and $a_g(\lambda)$ separation.

Figure 6 compares algorithm-derived $a(440)$ values versus true $a(440)$ values. These two algorithms process data at similar speeds (they take seconds to process a standard SeaWiFS image), but the error of the QAA is a factor of 3 smaller than that of the empirical algorithm for the entire $a(440)$ range [a factor of 5 smaller for $a(440) < 0.3\ m^{-1}$]. The two-band empirical algorithm[11] overestimated the $a(440)$ values, especially at the lower end. This could be because (1) the data set used for the algorithm development did not cover enough lower $a(440)$ points or (2) the $a(440)$ values used for the algorithm development, which were derived from the downwelling diffuse attenuation coefficient,[11] might still contain errors associated with the spectral variation of the average cosine for downwelling irradiance.[19] The comparison here, however, further emphasizes that performance of empirical algorithms depends on the consistency and accuracy of the data set used in the algorithm development, but the QAA presented here reduced that dependence.

Most of the $a(\lambda)$ error for the QAA-555 appears at the higher end of the data, which further leads to larger errors in $a_\phi(\lambda)$ and $a_g(\lambda)$ (see Fig. 5). This is for waters with higher chlorophyll or gelbstoff con-

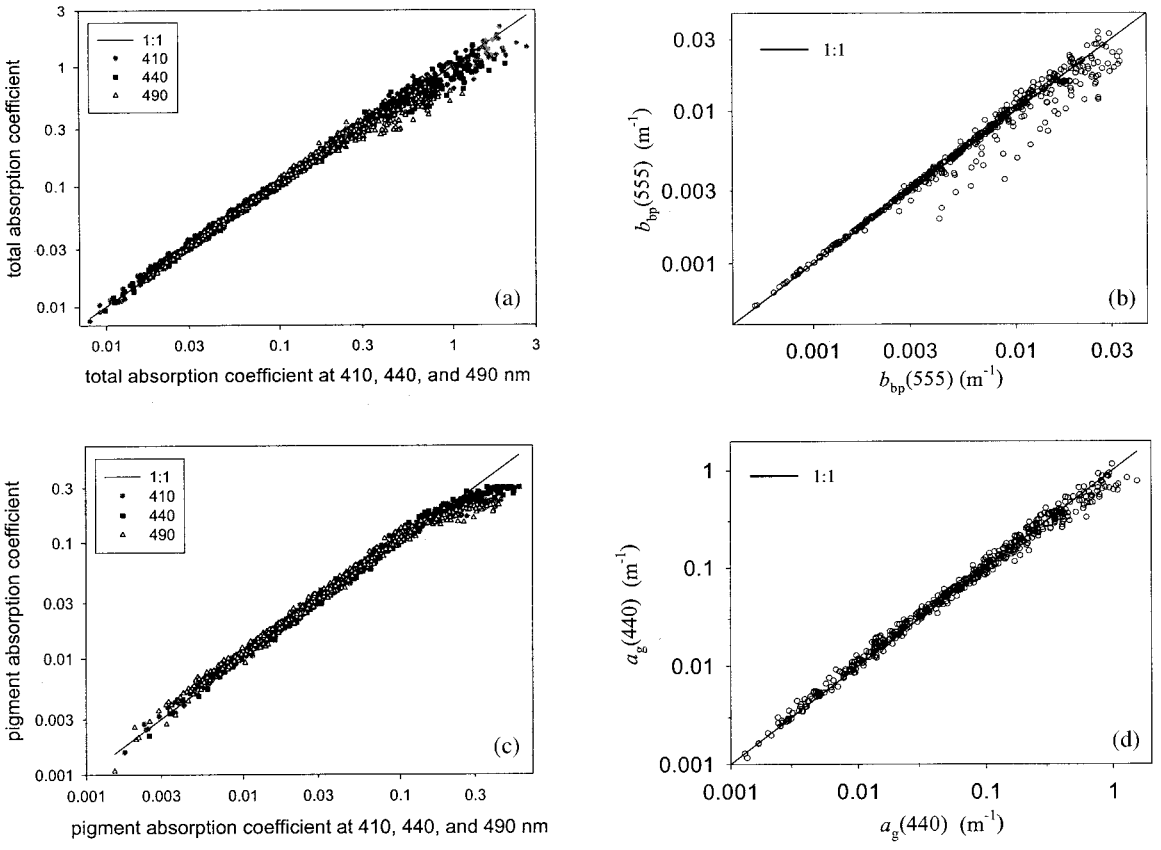


Fig. 5. Comparison of the QAA-555 derived values of (a) $a(\lambda)$, (b) $b_{bp}(555)$, (c) $a_\phi(\lambda)$, and (d) $a_g(440)$ versus their true values ($x$ axes) of the simulated data.

centrations, where the $a(555)$ values depart more from the values of pure water, and the empirically estimated $a(555)$ (step 2) are subject to larger errors when the water is less clear [see Fig. 4(a)].

For such higher-absorbing waters [$a(440) > 0.3$ m$^{-1}$], the reference wavelength needs to be shifted to a place longer than 555 nm, where pure-water absorption is still dominant even for larger $a_\phi(440)$ and $a_g(440)$ values. Assuming there is a band at 640 nm, this band is used as the reference wavelength. The analytical steps listed in Table 2 remain the same, but the estimation of $a(555)$ will be changed to the estimation of $a(640)$. Absorption of pure water at 640 nm is a factor of 5 larger than that at 555 nm, and the absorption of pigment and gelbstoff have limited contributions at 640 nm for most oceanic and coastal waters. As a result, the variation of $a(640)$ is even narrower than that of $a(555)$ (see Fig. 2). To estimate $a(640)$, step 2 is changed to

$$a(640) = 0.31 + 0.07\left[\frac{r_{rs}(640)}{r_{rs}(440)}\right]^{1.1}, \qquad (18)$$

with 0.31 in Eq. (18) the absorption coefficient of pure water at 640 nm.[53] The backscattering coefficient at 640 nm (step 3) is then calculated with known $u(640)$ and $a(640)$ values. $a(\lambda)$ is further calculated at step 6. With bands at 410 and 440 nm, $a_\phi(440)$ and $a_g(440)$ values are also calculated with the steps listed in Table 3.

Figure 7 presents the same comparisons as Fig. 5, but with retrievals by the QAA with 640 nm as the reference wavelength (QAA-640). $\varepsilon$ values are listed in Table 4. Clearly, for the higher-absorbing waters the QAA-640 performs better than the QAA-555, with similar performance at the lower-absorption end. This does not mean, however, that QAA-640 is al-

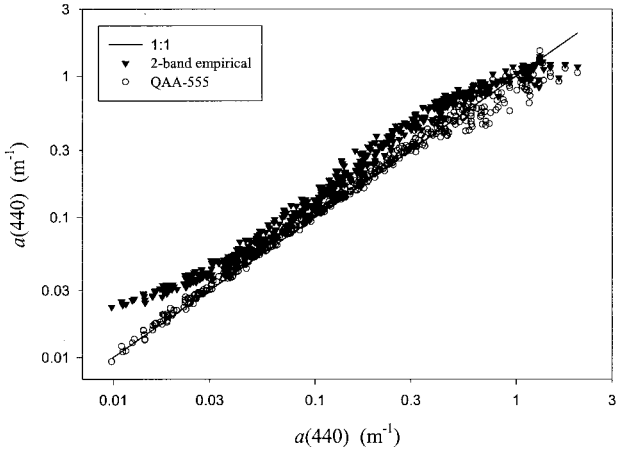


Fig. 6. Comparison of algorithm-retrieved $a(440)$ values versus true $a(440)$ values of the simulated data. The two-band empirical algorithm is from Lee *et al.*[11]

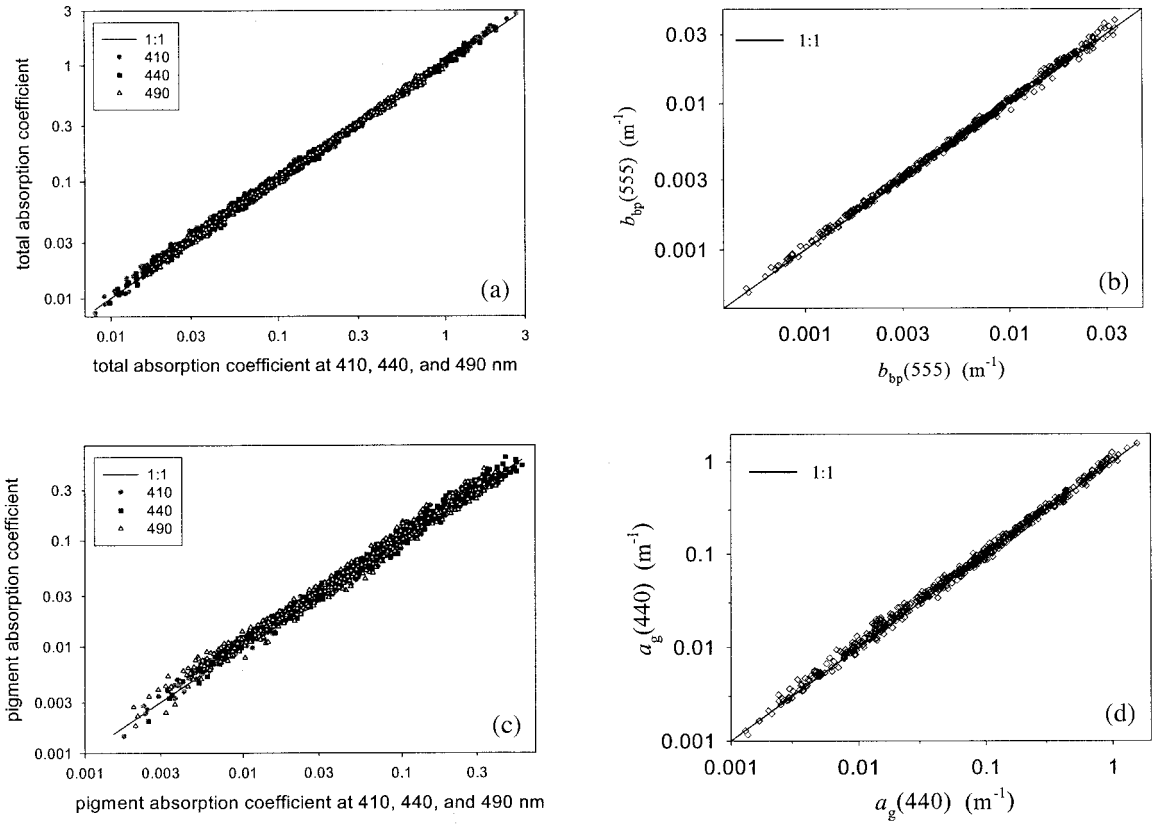


Fig. 7. Comparison of the QAA-640 derived values of (a) $a(\lambda)$, (b) $b_{bp}(555)$, (c) $a_\phi(\lambda)$, and (d) $a_g(440)$ versus their true values ($x$ axes) of the simulated data.

ways better than QAA-555. Because $a_w(640)$ is ~5 times that of $a_w(555)$, $r_{rs}(640)$ will be ~5 times smaller than $r_{rs}(555)$, which makes it more difficult to accurately measure $r_{rs}(640)$ than to measure $r_{rs}(555)$ for open-ocean waters, where $r_{rs}(640)$ is small. Therefore more errors could be introduced when QAA-640 is applied to open-ocean waters.

The errors are generally smaller for the four optical properties when we use a spectral optimization approach[34] (see Table 4). The spectral optimization used $r_{rs}$ values at all available wavelengths [QAA used only two bands for the derivation of the total absorption coefficient at 440 nm; more bands could be included to fine-tune the estimation of $a(\lambda_0)$], which improved retrieval accuracy at the higher-absorption end. Also, it is the same model for the pigment absorption coefficient used in the optimization and in the simulation, which helps to match the spectral shapes of the pigment absorption coefficient. If these shapes do not match each other closely, however, extra errors will be introduced to the optimization retrievals. Also, it must be kept in mind that optimization processing is time-consuming,[31] and currently it may take hours to process, for example, a standard SeaWiFS image.

When the QAA uses 640 nm as the reference wavelength, however, the difference between the accuracy of the QAA and the accuracy of the optimization is small. Also, if we ignore these high-end values but focus on the data with $a(440)$ less than 0.3 m$^{-1}$, then the ε value for $a(\lambda)$ is 8.2% by the QAA-555 and 5.9% by the optimization. It is encouraging that the QAA-555 provides equivalent results to those from the optimization algorithm for these clearer waters, suggesting that the QAA-555 could be used to process satellite data of such waters with results comparable to optimization processing.

Furthermore, if there is a band at 640 nm, the estimation for $a(555)$ can be greatly improved, at least for this data set, with

$$a(555) \approx 0.0596 + 0.56\left\{\left[\frac{r_{rs}(640)}{r_{rs}(555)}\right]^{1.7} - 0.03\right\}. \quad (19)$$

The $a(555)$ values from approximation (19) are shown in Fig. 4(a) (solid circles, 3.9% percentage error). After we replace the formula in step 2 with approximation (19) and derive $a(\lambda)$, $b_{bp}(\lambda)$, $a_\phi(\lambda)$, and $a_g(\lambda)$ values again using the steps listed in Tables 2 and 3, Fig. 8 compares them to their true values. Clearly all four properties are retrieved better than those shown in Fig. 5, with linear percentage errors of 6.5%, 7.3%, 12.7%, and 12.2% for $a(\lambda)$, $b_{bp}(555)$, $a_\phi(\lambda)$, and $a_g(440)$, respectively. This example indicates the possible areas for future improvement of the QAA.

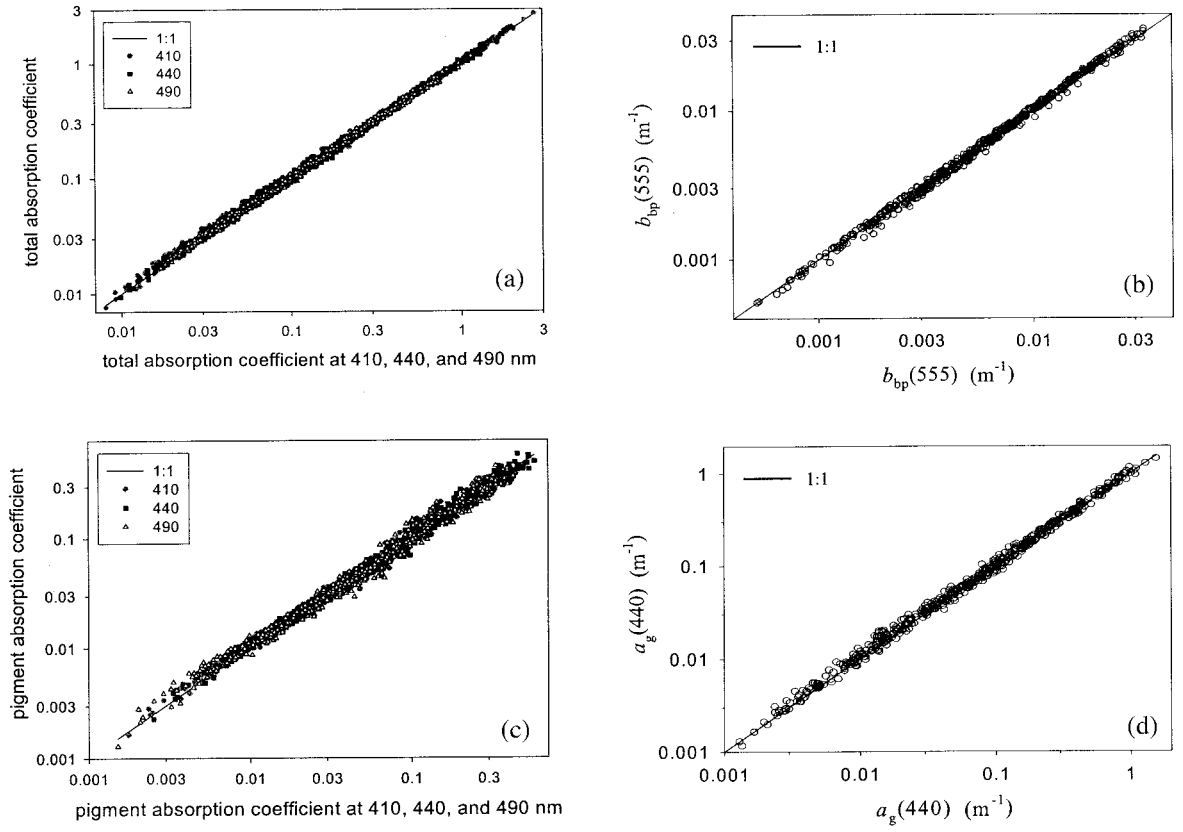


Fig. 8. Comparison of the QAA-555 derived values of (a) $a(\lambda)$, (b) $b_{bp}(555)$, (c) $a_{\phi}(\lambda)$, and (d) $a_g(440)$ versus their true values ($x$ axes) of the simulated data, after improved $a(555)$ estimation.

### B. Influence of Nonperfect Data

In the above, we used error-free data (perfect $r_{rs}$) to test the QAA. In the real world, $r_{rs}$ values will not be as good as the above because of measurement and atmospheric corrections. To see how the QAA performs for erroneous data, two tests were carried out. In test 1 we added $\pm 10\%$ random noise to the simulated $r_{rs}$ values at each wavelength and ran the QAA-555. In test 2 we increased all $r_{rs}$ values by 20% and again ran the QAA-555. This added noise could be viewed as errors to $r_{rs}$ introduced by imperfect sensor calibration or atmospheric correction. Figure 9 shows the results of test 1, and Fig. 10 shows the results of test 2. As above for perfect data, steps 2–6 in Table 2 were repeated once. For both tests, although the $r_{rs}$ values were perturbed, the QAA-555 still returned quite good $a(\lambda)$ estimates ($\varepsilon$ values are 19.5% for test 1 and 14.6% for test 2). Not surprisingly, the random noise has great influence on the decomposition of the total absorption into phytoplankton pigment [$\varepsilon = 57.0\%$ for $a_{\phi}(\lambda)$] and gelbstoff [$\varepsilon = 37.3\%$ for $a_g(440)$], whereas the 20% increase has more influence on the backscattering coefficient [$\varepsilon = 32.1\%$ for $b_{bp}(555)$]. The results of these tests further indicate that the QAA itself is quite noise tolerant to address field data, at least for the total absorption coefficient.

It is necessary to keep in mind that the above error analysis by use of the simulated data provides only a general guidance about the performance of the QAA. This is because (1) the simulated data cannot cover all the variations of the natural waters and (2) the expressions of Eqs. (13) and (14) may not be accurate in describing the responses of optical properties to biogeochemical properties of natural waters. As in any other algorithms, use of accurate field-measured data to test, validate, and improve the QAA should be done if we want to apply this QAA for oceanic observations.

### C. Field Data

Figure 11(a) compares the QAA-derived $a(\lambda)$ versus the AC9-measured $a(\lambda)$ for wavelengths at 410, 440, 490, and 530 nm. In the inversion process, $a(555)$ was estimated by approximation (19). For the four wavelengths, the $\varepsilon$ value is 12.5% and $r^2$ is 0.98 ($N = 80$), with the values from the AC9 slightly larger than the values from QAA. These values suggest that the two sets of results are in excellent agreement, and the differences are close to the accuracy limitations of each method itself. These results indicate that the true total absorption coefficients are near the ones from each process, although it is hard to know which set is closer to the truth as each method has its own sources of errors.

Figure 11(b) compares the QAA-derived $a(490)$ versus AC9-measured $a(490)$, along with the current SeaWiFS algorithm-derived $a(490)$. The SeaWiFS

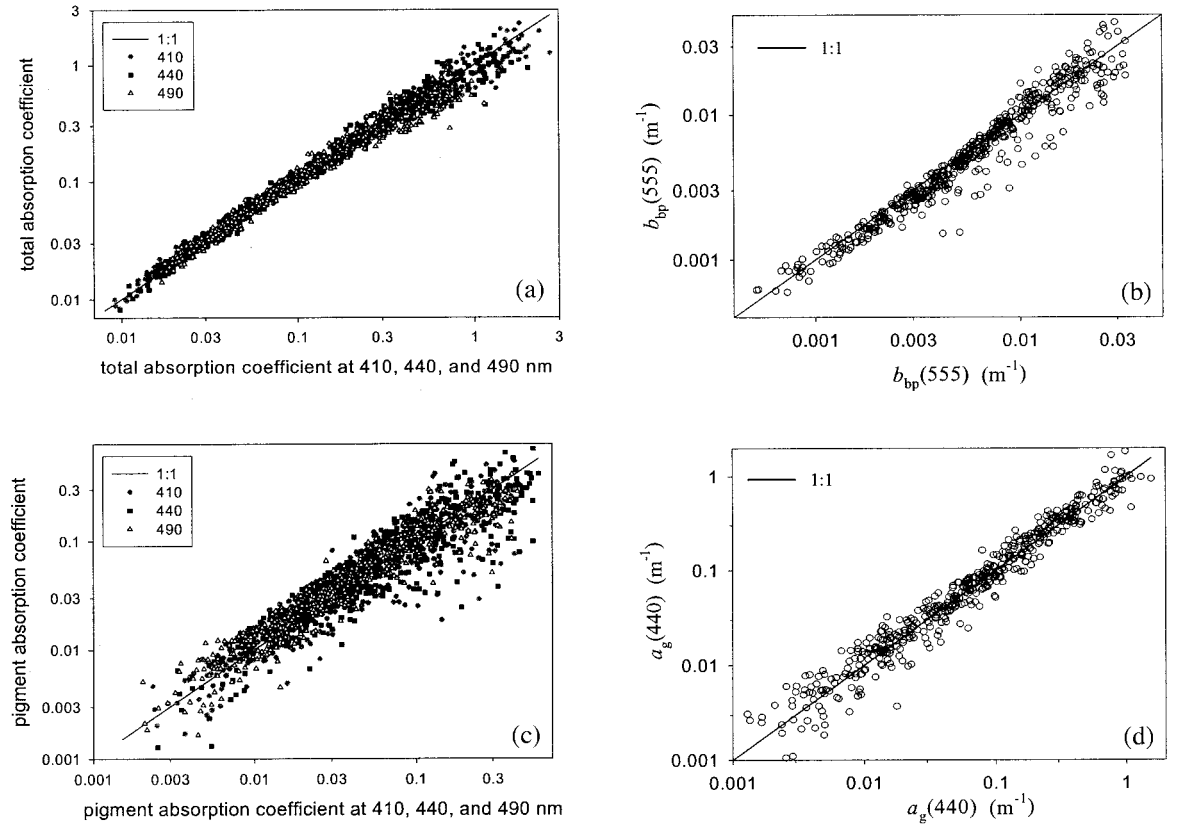


Fig. 9. Comparison of the QAA-555 derived values of (a) $a(\lambda)$, (b) $b_{bp}(555)$, (c) $a_\phi(\lambda)$, and (d) $a_g(440)$ versus their true values of the simulated data after $\pm 10\%$ random noise was added to the $r_{rs}$ values at each band.

$a(490)$ is converted from the SeaWiFS $K(490)$ [diffuse attenuation coefficient at 490 nm (Ref. 10)] after we applied the model of Morel,[54] with $K(490)$ derived empirically with the ratio of $r_{rs}(440)/r_{rs}(555)$.[10] Apparently the SeaWiFS $a(490)$ values are much larger at the higher end, whereas the QAA $a(490)$ is slightly smaller than the AC9 $a(490)$ (the $\varepsilon$ value is 9.8%). The larger SeaWiFS $a(490)$ at the higher end suggests that this algorithm needs to be adjusted for some of the turbid coastal waters. Note that the QAA process used $r_{rs}(640)$ values [in step 2 by approximation (19)], but the SeaWiFS process did not.

This field data set, however, is quite small and covers only a narrow range of natural waters, which is insufficient to completely validate the accuracy of the QAA, although the QAA was tested with the wide range of simulated data. More independent tests with field-measured data are desired and required for the validation and improvement of the QAA.

### D. Comparison with Optimization Results when Applied to Other Field Data

As an indirect test and consistency check of the performance of the QAA, it is applied to our earlier collected field data,[11] which covers a wider range of waters. The QAA-derived $a(\lambda)$ were compared with those from the spectral optimization. It is currently assumed that the optimization approach provides one of the best returns in ocean-color retrieval.[31] If the QAA is valid, its retrievals should be at least close to that from optimization to data not only from simulation but also from field measurements.

This field data came from a variety of oceanic and coastal environments with a wide range of water types, covering waters such as the West Florida Shelf, the Gulf of Mexico (including the Mississippi River plume), the Bering Sea, the Arabian Sea, the Sargasso Sea, and near Key West (Florida). Chlorophyll-$a$ concentrations ranged from 0.05 to 50.0 mg/m$^3$. Only optically deep waters were used. Locations and measurements for these data were documented in Lee *et al.*[11]

Figure 12(a) shows derived $a(440)$ values (in a range of 0.025–2.0 m$^{-1}$) from the QAA compared with those by use of full-spectrum optimization (400–800 nm with 5-nm spacing, 65 effective bands[28]). Clearly, as shown in the simulated data set, the QAA-555 provides almost identical results to those from optimization for $a(440)$ of less than 0.3 m$^{-1}$ ($\varepsilon$ = 7.3%), but underestimates $a(440)$ values when it gets larger ($\varepsilon$ = 16.9% for the entire range).

With 640 nm as the reference wavelength, the algorithm improves the estimates for higher $a(440)$ values, but performs less accurately at the lower $a(440)$ values. As discussed in Subsection 4.A, $r_{rs}(640)$ in the field are small for clearer waters and difficult to accurately measure. They can be further perturbed by nonperfect removal of surface-reflected skylight.

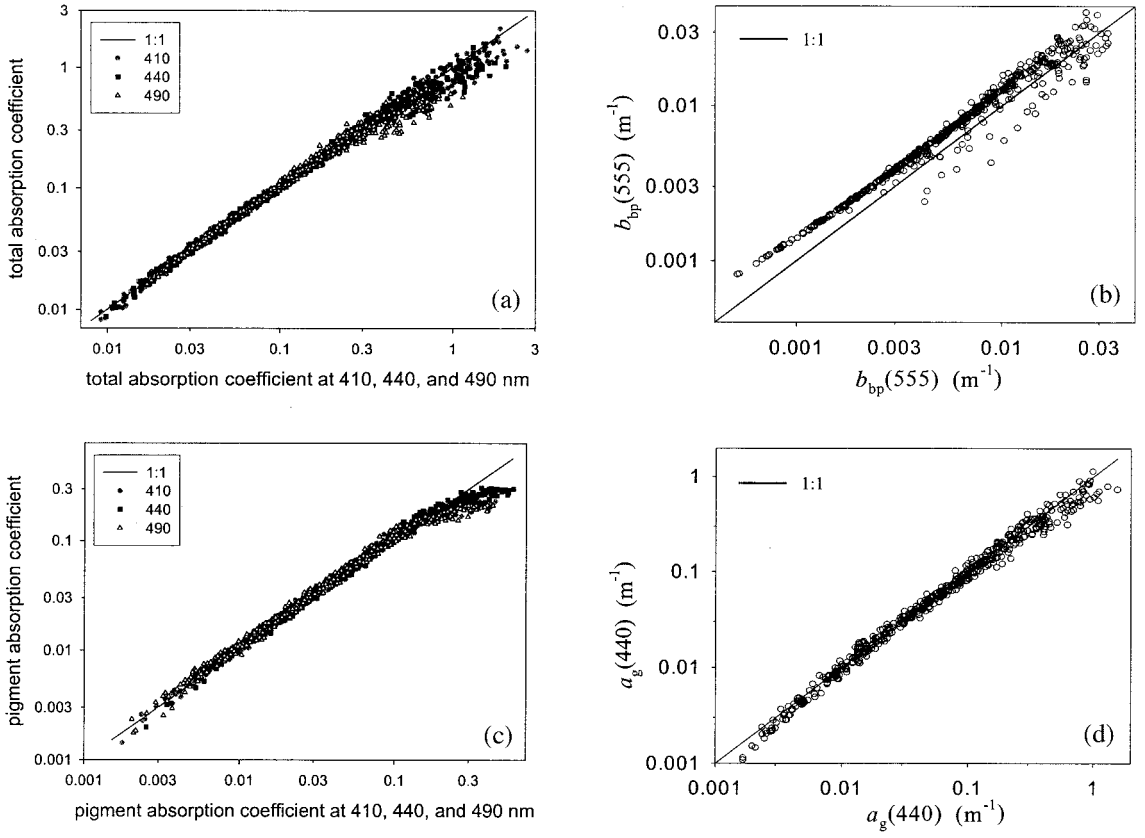


Fig. 10. Comparison of the QAA-555 derived values of (a) $a(\lambda)$, (b) $b_{bp}(555)$, (c) $a_\phi(\lambda)$, and (d) $a_g(440)$ versus their true values of the simulated data after a 20% increase to the $r_{rs}$ values at each band.

Also, the effects to $r_{rs}$ of Raman scattering are larger for clearer water at longer wavelengths.

These results suggest that a combination between the results of QAA-555 and that of QAA-640 can improve estimates for the entire range of this data set. Assuming that $a(\lambda)^{[555]}$ is the derived total absorption coefficient from the QAA-555 and that $a(\lambda)^{[640]}$ is the derived total absorption coefficient from the QAA-640, a combination of the two are

$$\begin{cases} a(\lambda) = a(\lambda)^{[555]}, & \text{for } a(440)^{[640]} < 0.2, \\ a(\lambda) = \left[\dfrac{0.3 - a(440)^{[640]}}{0.1}\right] a(\lambda)^{[555]} + \left[1 - \dfrac{0.3 - a(440)^{[640]}}{0.1}\right] a(\lambda)^{[640]}, & \text{for } 0.2 \le a(440)^{[640]} \le 0.3, \\ a(\lambda) = a(\lambda)^{[640]}, & \text{for } a(440)^{[640]} > 0.3. \end{cases} \quad (20)$$

Figure 12(b) shows the combined $a(\lambda)$ versus optimization-derived $a(\lambda)$, with an $\varepsilon$ value of 10.3%, suggesting that the two retrievals are consistent with each other. However, because the results from the spectral optimization also contain errors,[28,34] they cannot be used as standards to validate the accuracy of QAA.

There is no field-measured backscattering coefficient for comparison here. It needs to be pointed out that, when a remote-sensing reflectance model is applied in the field, because the actual shape of the particle phase function is not known, the differences between the used and required $g_0$ and $g_1$ values may be larger than the differences that appeared in the simulated data ($g_0$ and $g_1$ values are fixed in the inversion, but their values are somewhat random in the simulation). This mismatch can contribute as much as 20% extra error to the retrieval of the particle backscattering coefficients.[35,36,64] The mismatch has only limited influence, however, on the absorption coefficient, as absorption has no angular dependence. Therefore we should expect larger errors for estimates of $b_{bp}$ when applied to field data than those errors found for the simulated data.

Inelastic scattering such as Raman scattering and gelbstoff fluorescence are not considered in this study. Their effects can be corrected, however, to first order with proposed models[65–67] given knowledge of the absorption and backscattering coefficients

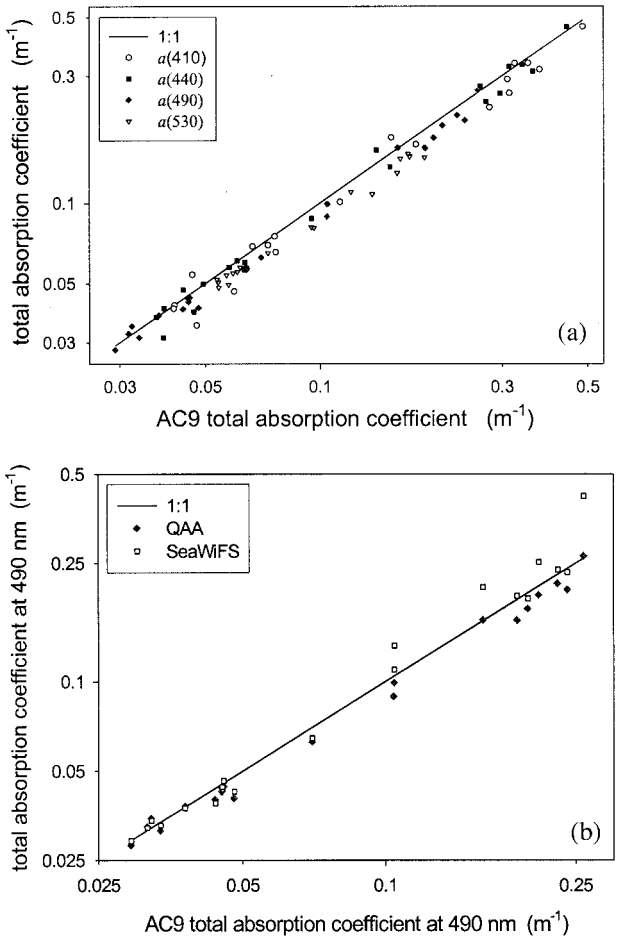


Fig. 11. (a) Comparison of the QAA-derived $a(\lambda)$ versus AC9-measured $a(\lambda)$ for field data. (b) For the same field data, comparison of the QAA-derived $a(490)$ versus AC9-measured $a(490)$, along with SeaWiFS algorithm-derived $a(490)$.

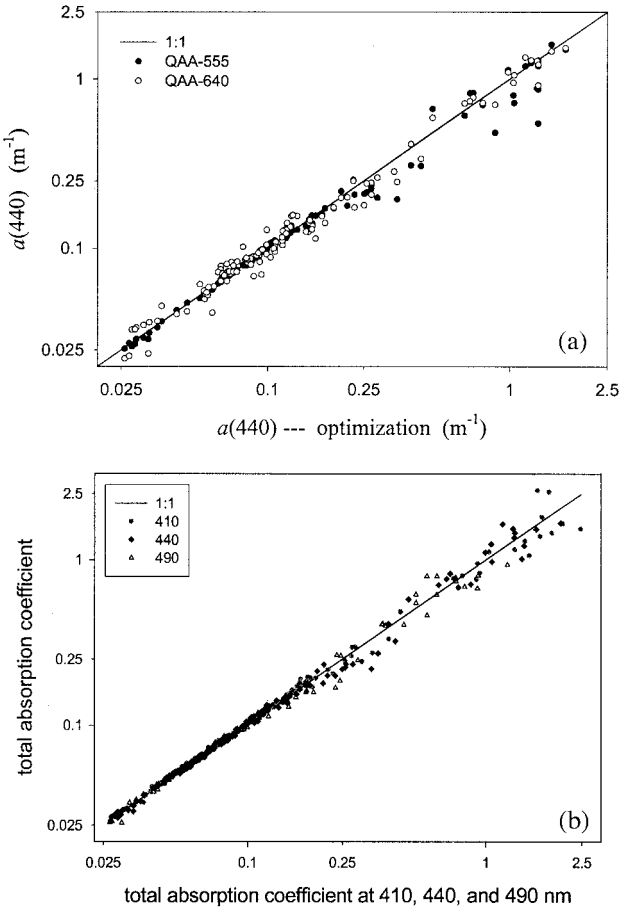


Fig. 12. (a) Comparison of the QAA-derived $a(440)$ versus optimization-derived $a(440)$ for earlier collected field data (see text for details). (b) Comparison of the QAA-derived $a(\lambda)$ versus optimization-derived $a(\lambda)$ ($x$ axes). QAA-$a(\lambda)$ is a combination of the results from QAA-555 and QAA-640.

of the water column. For sensors not viewing at nadir,[68] values of $T$, $g_0$, and $g_1$ need to be slightly adjusted. Without any correction, however, it is found that most of the errors will be transferred to the retrieved particle backscattering coefficient, with only little influence on the retrieved total absorption coefficient.[38]

## 5. Summary

For open-ocean and coastal waters, a multiband QAA is developed to retrieve total absorption and backscattering coefficients, as well as absorption coefficients of phytoplankton pigments and gelbstoff, from remote-sensing reflectance spectrum. The algorithm is based on relationships between remote-sensing reflectance and inherent optical properties of the water derived from the radiative transfer equation. For the derivation of total absorption and backscattering coefficients, there are no spectral models involved for pigment and gelbstoff absorption coefficients, which reduce model influences on the derived values. Furthermore, the near-analytical nature and the explicit step-by-step sequential calculation of the QAA make it easy to diagnose possible error sources in water-color inversion.

The algorithm uses multiband $r_{rs}$ values as inputs, and absorption and backscattering coefficients are calculated analytically from the values of $r_{rs}$. The algorithm can be applied to sensors with multispectral or hyperspectral bands as long as accurate $r_{rs}(\lambda)$ values are available. It can also be easily adapted for use of subsurface irradiance reflectance values as inputs for the calculations.

There are only two empirical aspects in the derivation of the total absorption and backscattering coefficients in the QAA. One relates to the estimation of the total absorption coefficient at a reference wavelength [$a(\lambda_0)$, as shown here $a(555)$ or $a(640)$]; the other relates to the estimation of the spectral slope ($Y$) of the particle backscattering coefficient. The reference wavelength is where $r_{rs}(\lambda_0)$ from elastic scattering can be well measured and $a(\lambda_0)$ can be well estimated. For $a(\lambda_0)$, because of its dominance by water absorption, errors are limited. Because few measurements of $Y$ are available, less is known about how $Y$ varies. Often in practice a smaller value (close to 0) is assumed for coastal waters, and a larger

value (around 2.0) is assumed for open-ocean waters.[13] Based on a field study, here we use a $r_{rs}(440)/r_{rs}(555)$ ratio to empirically estimate the $Y$ values.

To test the first part of the QAA (Table 2), we applied it to a simulated data set and a field data set, neither of which are $case_1$ dependent. For the simulated data set, the pigment concentration ranged from 0.03 to 30 $mg/m^3$, with the total absorption coefficient at 440 nm in a range of 0.01–2.0 $m^{-1}$. With the QAA-555, the percentage error for $a(\lambda)$ is 14.3% for the entire range and ~8% for $a(440) < 0.3$ $m^{-1}$. To the field data, the percentage difference for $a(\lambda)$ is 12.5% ($r^2 = 0.98, N = 80$) when compared with AC9-measured $a(\lambda)$.

We also applied the QAA to an earlier collected field data set to test its consistency versus the optimization results. We found that the percentage difference for $a(\lambda)$ is 10.3% for $a(\lambda)$ ranging from 0.025 to 2.3 $m^{-1}$ and it is just 6.9% for $a(440) < 0.3$ $m^{-1}$. These results suggest that the performance of the QAA is at least close to that of the optimization approach in the retrieval of total absorption coefficients from $r_{rs}$.

For less clear waters, a band around 640 nm as the reference wavelength is suggested for better retrievals. We used 640 nm here for the possible application to the MODIS sensor, which has a band at 645 nm. For future sensors such as the medium-resolution imaging spectrometer (MERIS) or the ocean-color imager, a band around 620 nm may work as well as the 640-nm band. For turbid river plume or coastal waters, it may be necessary to shift $\lambda_0$ to even longer wavelengths.

It is much more challenging to separate the phytoplankton absorption and gelbstoff absorption from the total absorption coefficient. For the separation, information regarding the spectral relations of the pigment and gelbstoff absorption at a few bands is required. With bands at 410 and 440 nm, the pigment and gelbstoff absorption coefficients are separated from the QAA-derived total absorption coefficient, after a simple empirical algorithm is employed for the ratio of $a_\phi(410)/a_\phi(440)$. For the simulated data here, the percentage error was 18% (10% for clearer waters) for $a_\phi(\lambda)$ and 18% (13% for clearer waters) for $a_g(440)$ when the QAA-555 was applied. More importantly, the separation of Tables 2 and 3 clearly indicates that the retrieval of the total absorption coefficients is independent of mathematical models for the absorption coefficients of phytoplankton pigments and gelbstoff.

The errors in the derived inherent optical properties here by the QAA are similar to those found by a full-spectrum optimization approach, but the computation time is dramatically reduced (hours to seconds when a standard SeaWiFS image is processed), which makes it suitable to process large data sets such as satellite images.

We are in debt to Andrew Barnard for his AC9 data and grateful for the comments and suggestions from Jennifer Cannizzaro and the two anonymous reviewers. Financial support was provided by the following contracts and grants: NASA grants NAS5-97137, NAS5-31716, and NAG5-3446; the U.S. Office of Naval Research grants N00014-96-I-5013 and N00014-97-0006; and the National Oceanic and Atmospheric Administration Coastal Ocean Program R/NCOP-5.

## References

1. R. W. Preisendorfer, *Introduction*, Vol. 1 of Hydrologic Optics, NTIS PB-259 793/8ST (National Technical Information Service, Springfield, Ill., 1976).
2. H. R. Gordon and A. Morel, *Remote Assessment of Ocean Color for Interpretation of Satellite Visible Imagery: A Review*, R. T. Barber, C. N. K. Mooers, M. J. Bowman, and B. Zeitzschel, eds. (Springer-Verlag, New York, 1983).
3. N. G. Jerlov, *Marine Optics*, Vol. 14 of Elsevier Oceanography Series (Elsevier, New York, 1976).
4. K. L. Carder, P. Reinersman, R. F. Chen, F. Mueller-Karger, C. O. Davis, and M. Hamilton, "AVIRIS calibration and application in coastal oceanic environments," Remote Sens. Environ. **44,** 205–216 (1993).
5. R. P. Stumpf and J. R. Pennock, "Remote estimation of the diffuse attenuation coefficient in a moderately turbid estuary," Remote Sens. Environ. **38,** 183–191 (1991).
6. IOCCG, *Status and Plans for Satellite Ocean-Color Missions: Considerations for Complementary Missions*, J. Yoder, ed., Reports of the International Ocean-Colour Coordinating Group, No. 2 (IOCCG, Dartmouth, Nova Scotia, Canada, 1998).
7. A. Morel and L. Prieur, "Analysis of variations in ocean color," Limnol. Oceanogr. **22,** 709–722 (1977).
8. R. W. Austin and T. J. Petzold, "The determination of the diffuse attenuation coefficient of sea water using the coastal zone color scanner," in *Oceanography from Space*, J. F. R. Gower, ed. (Plenum, New York, 1981), pp. 239–256.
9. H. R. Gordon, D. K. Clark, J. W. Brown, O. B. Brown, R. H. Evans, and W. W. Broenkow, "Phytoplankton pigment concentrations in the Middle Atlantic Bight: comparison of ship determinations and CZCS estimates," Appl. Opt. **22,** 20–36 (1983).
10. J. L. Mueller and C. C. Trees, "Revised SeaWIFS prelaunch algorithm for diffuse attenuation coefficient K(490)," in *Case Studies for SeaWiFS Calibration and Validation*, NASA Tech Memo. 104566, Vol. 41, S. B. Hooker and E. R. Firestone, eds. (NASA Goddard Space Flight Center, Greenbelt, Md., 1997), pp. 18–21.
11. Z. P. Lee, K. L. Carder, R. G. Steward, T. G. Peacock, C. O. Davis, and J. S. Patch, "An empirical algorithm for light absorption by ocean water based on color," J. Geophys. Res. **103,** 27967–27978 (1998).
12. R. Doerffer and H. Schiller, "Determination of Case 2 water constituents using radiative transfer simulation and its inversion by neural networks," in *Proceedings of Ocean Optics XIV*, S. G. Ackleson and J. Campbell, eds. (U.S. Office of Naval Research, Washington, D.C., 1998).
13. S. Sathyendranath, L. Prieur, and A. Morel, "A three-component model of ocean color and its application to remote sensing of phytoplankton pigments in coastal waters," Int. J. Remote Sens. **10,** 1373–1394 (1989).
14. F. E. Hoge and R. N. Swift, "Chlorophyll pigment concentration using spectral curvature algorithms: an evaluation of present and proposed satellite ocean color sensor bands," Appl. Opt. **25,** 3677–3682 (1986).
15. S. Sathyendranath, F. E. Hoge, T. Platt, and R. N. Swift, "Detection of phytoplankton pigments from ocean color: improved algorithms," Appl. Opt. **33,** 1081–1089 (1994).

16. J. O'Reilly, S. Maritorena, B. G. Mitchell, D. Siegel, K. L. Carder, S. Garver, M. Kahru, and C. McClain, "Ocean color chlorophyll algorithms for SeaWiFS," J. Geophys. Res. **103,** 24937–24953 (1998).
17. M. X. He, Z. S. Liu, K. P. Du, L. P. Li, R. Chen, K. L. Carder, and Z. P. Lee, "Retrieval of chlorophyll from remote-sensing reflectance in the China Seas," Appl. Opt. **39,** 2467–2474 (2000).
18. M. Kahru and B. G. Mitchell, "Empirical chlorophyll algorithm and preliminary SeaWiFS validation for the California Current," Int. J. Remote Sens. **20,** 3423–3429 (1999).
19. H. Loisel, D. Stramski, B. G. Mitchell, F. Fell, V. Fournier-Sicre, B. Lemasle, and M. Babin, "Comparison of the ocean inherent optical properties obtained from measurements and inverse modeling," Appl. Opt. **40,** 2384–2397 (2001).
20. M. Sydor, R. Arnone, R. W. Gould, G. E. Terrie, S. D. Ladner, and C. G. Wood, "Remote-sensing technique for determination of the volume absorption coefficient of turbid water," Appl. Opt. **37,** 4944–4950 (1998).
21. R. W. Gould, R. A. Arnone, and M. Sydor, "Absorption, scattering, and remote-sensing reflectance relationships in coastal waters: testing a new inversion algorithm," J. Coastal Res. **17,** 328–341 (2001).
22. S. Sathyendranath, G. Cota, V. Stuart, M. Maass, and T. Platt, "Remote sensing of phytoplankton pigments: a comparison of empirical and theoretical approaches," Int. J. Remote Sens. **22,** 249–273 (2001).
23. R. P. Bukata, J. H. Jerome, K. Y. Kondratyev, and D. V. Pozdnyakov, *Optical Properties and Remote Sensing of Inland and Coastal Waters* (CRC Press, Boca Raton, Fla., 1995).
24. R. Doerffer and J. Fisher, "Concentrations of chlorophyll, suspended matter, and gelbstoff in case II waters derived from satellite coastal zone color scanner data with inverse modeling methods," J. Geophys. Res. **99,** 7475–7466 (1994).
25. F. E. Hoge and P. E. Lyon, "Satellite retrieval of inherent optical properties by linear matrix inversion of oceanic radiance models: an analysis of model and radiance measurement errors," J. Geophys. Res. **101,** 16631–16648 (1996).
26. K. L. Carder, F. R. Chen, Z. P. Lee, S. K. Hawes, and D. Kamykowski, "Semianalytic Moderate-Resolution Imaging Spectrometer algorithms for chlorophyll-a and absorption with bio-optical domains based on nitrate-depletion temperatures," J. Geophys. Res. **104,** 5403–5421 (1999).
27. C. S. Roesler and M. J. Perry, "In situ phytoplankton absorption, fluorescence emission, and particulate backscattering spectra determined from reflectance," J. Geophys. Res. **100,** 13279–13294 (1995).
28. Z. P. Lee, K. L. Carder, T. G. Peacock, C. O. Davis, and J. L. Mueller, "Method to derive ocean absorption coefficients from remote-sensing reflectance," Appl. Opt. **35,** 453–462 (1996).
29. S. A. Garver and D. Siegel, "Inherent optical property inversion of ocean color spectra and its biogeochemical interpretation. 1. Time series from the Sargasso Sea," J. Geophys. Res. **102,** 18607–18625 (1997).
30. A. H. Barnard, J. R. Zaneveld, and W. S. Pegau, "*In situ* determination of the remotely sensed reflectance and the absorption coefficient: closure and inversion," Appl. Opt. **38,** 5108–5117 (1999).
31. IOCCG, *Remote Sensing of Ocean Colour in Coastal, and Other Optically Complex, Waters*, S. Sathyendranath, ed., Reports of the International Ocean-Colour Coordinating Group, No. 3 (IOCCG, Dartmouth, Nova Scotia Canada, 2000).
32. Z. P. Lee, K. L. Carder, J. Marra, R. G. Steward, and M. J. Perry, "Estimating primary production at depth from remote sensing," Appl. Opt. **35,** 463–474 (1996).
33. H. R. Gordon, O. B. Brown, R. H. Evans, J. W. Brown, R. C. Smith, K. S. Baker, and D. K. Clark, "A semi-analytic radiance model of ocean color," J. Geophys. Res. **93,** 10909–10924 (1988).
34. Z. P. Lee, K. L. Carder, C. D. Mobley, R. G. Steward, and J. S. Patch, "Hyperspectral remote sensing for shallow waters. 2. Deriving bottom depths and water properties by optimization," Appl. Opt. **38,** 3831–3843 (1999).
35. A. Morel and B. Gentili, "Diffuse reflectance of oceanic waters. II. Bidirectional aspects," Appl. Opt. **32,** 6864–6879 (1993).
36. J. R. V. Zaneveld, "Remotely sensed reflectance and its dependence on vertical structure: a theoretical derivation," Appl. Opt. **21,** 4146–4150 (1982).
37. J. H. Jerome, R. P. Bukata, and J. R. Miller, "Remote sensing reflectance and its relationship to optical properties of natural waters," Int. J. Remote Sens. **17,** 3135–3155 (1996).
38. Z. P. Lee and K. L. Carder, "Particle phase function and remote-sensing reflectance model: a revisit," presented at the Ocean Color Research Team Meeting, San Diego, Calif., 21–24 May 2001.
39. D. Stramski and D. A. Kiefer, "Optical properties of marine bacteria," in *Ocean Optics X*, R. W. Spinrad, ed., Proc. SPIE **1302,** 250–268 (1990).
40. X. D. Zhang, M. Lewis, and B. Johnson, "Influence of bubbles on scattering of light in the ocean," Appl. Opt. **37,** 6525–6536 (1998).
41. A. Morel, "Optical properties of pure water and pure sea water," in *Optical Aspects of Oceanography*, N. G. Jerlov and E. S. Nielsen, eds. (Academic, New York, 1974), pp. 1–24.
42. H. R. Gordon, R. C. Smith, and J. R. V. Zaneveld, "Introduction to ocean optics," in *Ocean Optics VI*, S. Q. Duntley, ed., Proc. SPIE **208,** 1–43 (1980).
43. R. C. Smith and K. S. Baker, "Optical properties of the clearest natural waters," Appl. Opt. **20,** 177–184 (1981).
44. C. D. Mobley, *Light and Water: Radiative Transfer in Natural Waters* (Academic, New York, 1994).
45. C. D. Mobley, *Hydrolight 3.0 Users' Guide*, Final Report (SRI International, Menlo Park, Calif., 1995).
46. Z. P. Lee, K. L. Carder, R. G. Steward, T. G. Peacock, C. O. Davis, and J. L. Mueller, "Remote-sensing reflectance and inherent optical properties of oceanic waters derived from above-water measurements," in *Ocean Optics XIII*, S. G. Ackleson, ed., Proc. SPIE **2963,** 160–166 (1996).
47. Z. P. Lee, "Visible-infrared remote-sensing model and applications for ocean waters," Ph.D. dissertation (Department of Marine Science, University of South Florida, St. Petersburg, Fla., 1994).
48. A. Bricaud, M. Babin, A. Morel, and H. Claustre, "Variability in the chlorophyll-specific absorption coefficients of natural phytoplankton: analysis and parameterization," J. Geophys. Res. **100,** 13321–13332 (1995).
49. A. Bricaud, A. Morel, and L. Prieur, "Absorption by dissolved organic matter of the sea (yellow substance) in the UV and visible domains," Limnol. Oceanogr. **26,** 43–53 (1981).
50. N. Hoepffner and S. Sathyendranath, "Effect of pigment composition on absorption properties of phytoplankton," Mar. Ecol. Prog. Ser. **73,** 11–23 (1991).
51. K. L. Carder, R. G. Steward, G. R. Harvey, and P. B. Ortner, "Marine humic and fulvic acids: their effects on remote sensing of ocean chlorophyll," Limnol. Oceanogr. **34,** 68–81 (1989).
52. K. L. Carder, S. K. Hawes, K. A. Baker, R. C. Smith, R. G. Steward, and B. G. Mitchell, "Reflectance model for quantifying chlorophyll *a* in the presence of productivity degradation products," J. Geophys. Res. **96,** 20599–20611 (1991).
53. R. Pope and E. Fry, "Absorption spectrum (380–700 nm) of pure waters: II. Integrating cavity measurements," Appl. Opt. **36,** 8710–8723 (1997).
54. A. Morel, "Optical modeling of the upper ocean in relation to its biogenous matter content (Case I waters)," J. Geophys. Res. **93,** 10749–10768 (1988).

55. A. Morel and S. Maritorena, "Bio-optical properties of oceanic waters: a reappraisal," J. Geophys. Res. **106,** 7163–7180 (2001).
56. Z. P. Lee, K. L. Carder, C. D. Mobley, R. G. Steward, and J. S. Patch, "Hyperspectral remote sensing for shallow waters. 1. A semianalytical model," Appl. Opt. **37,** 6329–6338 (1998).
57. K. L. Carder and R. G. Steward, "A remote-sensing reflectance model of a red tide dinoflagellate off West Florida," Limnol. Oceanogr. **30,** 286–298 (1985).
58. J. L. Mueller, San Diego State University Center for Hydro-Optics and Remote Sensing, and SIMBIOS Science Team, *Ocean Optics Protocols for Satellite Ocean Color Sensor Validation*, Rev. 3, NASA Tech. Memo 210004 J. L. Mueller and G. S. Fargion, eds. (NASA Goddard Space Flight Center, Greenbelt, Md., 2002), Vols. 1 and 2.
59. W. S. Pegau, J. S. Cleveland, W. Doss, C. D. Kennedy, R. A. Maffione, J. L. Mueller, R. Stone, C. C. Trees, A. D. Weidemann, W. H. Wells, and J. R. V. Zaneveld, "A comparison of methods for the measurement of the absorption coefficient in natural waters," J. Geophys. Res. **100,** 13201–13220 (1995).
60. For more details on the AC9, see http://www.wetlabs.com/publac9.
61. H. R. Gordon and W. R. McCluney, "Estimation of the depth of sunlight penetration in the sea for remote sensing," Appl. Opt. **14,** 413–416 (1975).
62. H. R. Gordon, "Diffuse reflectance of the ocean: influence of nonuniform phytoplankton pigment profile," Appl. Opt. **31,** 2116–2129 (1992).
63. Z. P. Lee, K. L. Carder, R. F. Chen, and T. G. Peacock, "Properties of the water column and bottom derived from AVIRIS data," J. Geophys. Res. **106,** 11639–11652 (2001).
64. R. H. Stavn and A. D. Weidemann, "Shape factors, two-flow models, and the problem of irradiance inversion in estimating optical parameters," Limnol. Oceanogr. **34,** 1426–1441 (1989).
65. Z. P. Lee, K. L. Carder, S. K. Hawes, R. G. Steward, T. G. Peacock, and C. O. Davis, "Model for interpretation of hyperspectral remote sensing reflectance," Appl. Opt. **33,** 5721–5732 (1994).
66. S. K. Hawes, "Quantum fluorescence efficiencies of marine fulvic and humic acids," M.S. thesis (Department of Marine Science, University of South Florida, St. Petersburg, Fla., 1992).
67. S. Sathyendranath and T. Platt, "Ocean-color model incorporating transpectral processes," Appl. Opt. **37,** 2216–2227 (1998).
68. A. Morel and B. Gentili, "Diffuse reflectance of oceanic waters. III. Implications of bidirectionality for the remote-sensing problem," Appl. Opt. **35,** 4850–4862 (1996).